Observation of the decays χ cJ → nKS0Λ¯ + c.c.

BESIII Collaboration; Kalantar-Nayestanaki, N.; Kappert, R.; Kavatsyuk, M.; Messchendorp, Johan; Rodin, V.

Published in:
Journal of High Energy Physics

DOI:
10.1007/JHEP11(2021)217

Publication date:
2021

Published for SISSA by Springer

Received: June 28, 2021
Revised: September 18, 2021
Accepted: November 13, 2021
Published: November 29, 2021

JHEP11(2021)217

Observation of the decays $\chi_{cJ} \to nK^0_S\bar{\Lambda} + \text{c.c.}$

BESIII

The BESIII collaboration

E-mail: besiii-publications@ihep.ac.cn

Abstract: By analyzing 4.48×10^8 $\psi(3686)$ events collected with the BESIII detector, we observe the decays $\chi_{cJ} \to nK^0_S\bar{\Lambda} + \text{c.c.}$ ($J = 0, 1, 2$) for the first time, via the radiative transition $\psi(3686) \to \gamma\chi_{cJ}$. The branching fractions are determined to be $(6.65 \pm 0.26_{\text{stat}} \pm 0.41_{\text{syst}}) \times 10^{-4}$, $(1.66 \pm 0.12_{\text{stat}} \pm 0.12_{\text{syst}}) \times 10^{-4}$, and $(3.58 \pm 0.16_{\text{stat}} \pm 0.23_{\text{syst}}) \times 10^{-4}$ for $J = 0$, 1, and 2, respectively.

Keywords: e^+-e^- Experiments

ArXiv ePrint: 2106.13442

https://doi.org/10.1007/JHEP11(2021)217

Contents

JHEP11(2021)217

1 Introduction

Studying the hadronic decays of the $c\bar{c}$ states J/ψ, $\psi(3686)$, and χ_{cJ} ($J = 0, 1, 2$) provides valuable information on perturbative QCD in the charmonium-mass regime and on the structure of charmonia. The color-octet mechanism, which successfully describes several decay patterns of P-wave χ_{cJ} states [1], may be applicable to further χ_{cJ} decays. Measurements of χ_{cJ} hadronic decays can provide a test of the color-octet mechanism and further assist in understanding χ_{cJ} decay mechanisms.

The BES collaboration observed near-threshold structures in baryon-antibaryon invariant mass distributions in the radiative decay $J/\psi \to \gamma p\bar{p}$ [2] and the purely hadronic decay $J/\psi \to pK^-\bar{\Lambda}$ [3]. It was suggested theoretically that these near-threshold structures might be observation of baryonium [4–6] or caused by final state interactions [7–9]. Excited Λ and N resonances were observed in the study of the decay $J/\psi \to nK^0_S\bar{\Lambda}$ [10]. Studying the same decay modes in other charmonia can provide complementary information on these structures.

Anomalous enhancements near the threshold of $p\bar{\Lambda}$ + c.c. have been also observed in the decays $\chi_{cJ} \to pK^-\bar{\Lambda}$ + c.c. by the BESIII collaboration [11]. If isospin symmetry is conserved, the decay branching fraction (BF) ratio $\mathcal{B}(\chi_{cJ} \to pK^-\bar{\Lambda} + \text{c.c.})/\mathcal{B}(\chi_{cJ} \to nK^0_S\bar{\Lambda}+\text{c.c.}) \sim 2$ should be satisfied, thereby implying the existence of the isospin conjugate

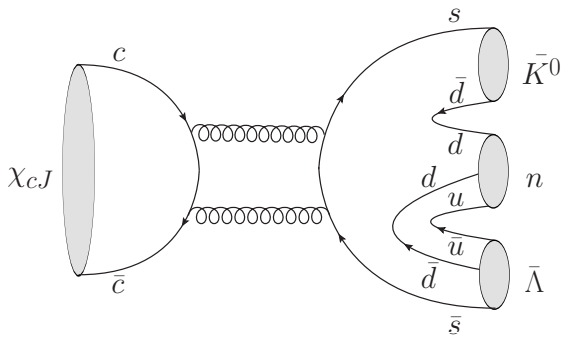

Figure 1. Feynman diagram of the $\chi_{cJ} \to nK_S^0\bar{\Lambda}$ decay, where $J = 0$, 1, and 2.

decays $\chi_{cJ} \to nK_S^0\bar{\Lambda}$ + c.c. and providing predictions for their BFs. A typical diagram for the decay is shown in figure 1.

In this analysis, we present the study of $\chi_{cJ} \to nK_S^0\bar{\Lambda}$ + c.c. using the $\psi(3686)$ data sample containing $(4.48 \pm 0.03) \times 10^8$ events collected at BESIII [12]. The radiative decays $\psi(3686) \to \gamma\chi_{cJ}$, which have a BF of approximately 10% for each χ_{cJ} [13], offer an ideal environment to investigate χ_{cJ} decays. Throughout this paper, charge conjugate modes are implied unless otherwise stated.

2 Detector and data sets

The BESIII detector is a magnetic spectrometer [14, 15] located at the Beijing Electron Positron Collider (BEPCII) [16]. The cylindrical core of the BESIII detector consists of a helium-based multilayer drift chamber (MDC), a plastic scintillator time-of-flight system (TOF), and a CsI (Tl) electromagnetic calorimeter (EMC), which are all enclosed in a superconducting solenoidal magnet providing a 1.0 T magnetic field. The solenoid is supported by an octagonal flux-return yoke with resistive plate counter muon identifier modules interleaved with steel. The acceptance of charged particles and photons is 93% over 4π solid angle. The charged-particle momentum resolution at 1.0 GeV/c is 0.5%, and the specific energy loss (dE/dx) resolution is 6% for the electrons from Bhabha scattering. The EMC measures photon energies with a resolution of 2.5% (5%) at 1 GeV in the barrel (end cap) region. The time resolution of the TOF barrel part is 68 ps, while that of the end cap part is 110 ps.

Simulated samples produced with the GEANT4-based [17] Monte-Carlo (MC) software, which includes the geometric description of the BESIII detector and the detector response, are used to determine the detection efficiencies and to estimate the background levels. The simulation takes into account the beam energy spread and initial state radiation (ISR) in the e^+e^- annihilation modeled with the generator KKMC [18]. The inclusive MC samples consist of 5.06×10^8 $\psi(3686)$ events, the ISR production of the J/ψ state, and the continuum processes incorporated in KKMC. The known decay modes are modeled with EVENTGEN [19] using the BFs taken from the Particle Data Group (PDG) [13], and the remaining unknown

JHEP11(2021)217

decays of charmonium states from LUNDCHARM [20]. Radiation from charged final state particles is incorporated with the PHOTOS [21] package.

The signal detection efficiencies are estimated with signal MC samples. The decays of $\psi(3686) \to \gamma\chi_{cJ}$ ($J = 0, 1, 2$) are simulated following ref. [22], in which the magnetic-quadrupole (M2) transition for $\psi(3686) \to \gamma\chi_{c1,2}$ and the electric-octupole (E3) transition for $\psi(3686) \to \gamma\chi_{c2}$ are considered in addition to the dominant electric-dipole (E1) transition. For the decay $\chi_{cJ} \to nK^0_S\bar{\Lambda}$ + c.c., a special generator based on results of Helicity Partial Wave Analysis (HelPWA) [23–25] is used (see appendix A). The background MC samples are obtained from inclusive MC samples, in which the signal channels are removed with TopoAna [26], and the samples are normalized to the data sample based on luminosity.

3 Event selection and background analysis

The signal process $\psi(3686) \to \gamma\chi_{cJ}, \chi_{cJ} \to nK^0_S\bar{\Lambda}$ with $K^0_S \to \pi^+\pi^-$ and $\bar{\Lambda} \to \bar{p}\pi^+$ consists of the final state particles $\gamma n\bar{p}\pi^+\pi^+\pi^-$. Charged track candidates from the MDC must satisfy $|\cos\theta| < 0.93$, where θ is the polar angle with respect to the z axis, which is the axis of the MDC. The closest approach to the interaction point is required to be less than 20 cm along the z direction and less than 10 cm in the plane perpendicular to z. The TOF and dE/dx information are combined to calculate the particle identification probabilities (P) for the hypotheses that a track is a pion, kaon, or proton. Proton candidates are required to satisfy $P(p) > P(K)$ and $P(p) > P(\pi)$. Exactly four charged tracks are required in each candidate event.

Since K^0_S and $\bar{\Lambda}$ have relatively long lifetimes, they are reconstructed by constraining the $\pi^+\pi^-$ pair and the $\bar{p}\pi^+$ pair to originate from secondary vertices, respectively. Charged track candidates, except the one used as a $\bar{p}$ in the $\bar{\Lambda}$ reconstruction, are assumed to be pions without applying particle identification. The decay lengths of K^0_S and $\bar{\Lambda}$ from the secondary vertex fits divided by their corresponding uncertainties are required to be larger than two. The mass distributions of the reconstructed K^0_S (denoted as $M_{\pi\pi}$) and $\bar{\Lambda}$ (denoted as $M_{\bar{p}\pi^+}$) candidates are shown in figures 2(a) and 2(b), respectively, where the signal regions are defined as $[0.480, 0.516]\,\mathrm{GeV}/c^2$ for K^0_S and $[1.112, 1.120]\,\mathrm{GeV}/c^2$ for $\bar{\Lambda}$.

Photons are reconstructed as energy clusters in the EMC. The shower time is required to be within $[0, 700]$ ns from the event start time. Photon candidates within $|\cos\theta| < 0.80$ (barrel) are required to have deposited energies larger than 25 MeV and those with $0.86 < |\cos\theta| < 0.92$ (end caps) must have deposited energies larger than 50 MeV. The photon candidates must be at least 10° away from any charged track to suppress Bremsstrahlung photons or splitoffs. We require at least one photon candidate satisfying the above criteria.

A 1-C kinematic fit is applied under the hypothesis of $\psi(3686) \to \gamma nK^0_S\bar{\Lambda}$ to select the best combination and to improve the resolution, where the neutron is treated as a missing particle. The value of $\chi^2_{\rm 1C}$ is required to be less than 200. If more than one combination survives in an event, the one with the smallest $\chi^2_{\rm 1C}$ is retained.

The invariant mass of the four momentum of the missing particle, $M_{\rm miss}$, is defined as $p_{\rm miss} = p_{\rm CM} - p_\gamma - p_{K^0_S} - p_\Lambda$, where p_i is the four momentum of the particle i and $p_{\rm CM}$ is the four momentum of the initial e^+e^- system. To further improve the purity, $M_{\rm miss}$ before

JHEP11(2021)217

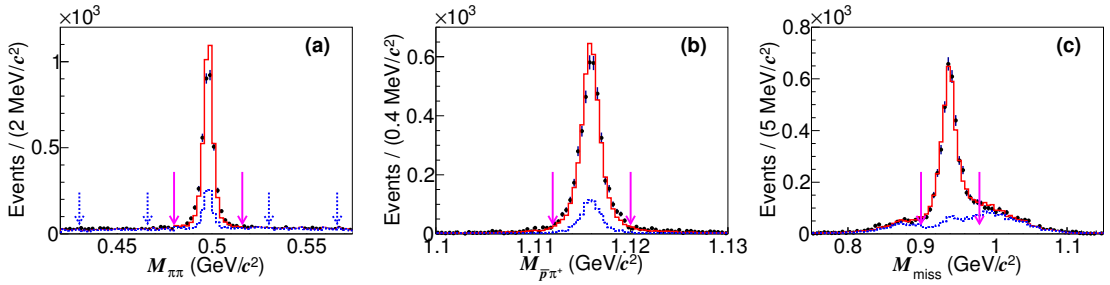

Figure 2. Distributions of (a) $M_{\pi\pi}$ of the K^0_S candidates, (b) $M_{\bar{p}\pi^+}$ of the $\bar{\Lambda}$ candidates, and (c) $M_{\rm miss}$ before the 1-C kinematic fit. Dots with error bars are data. Red solid (blue dashed) lines refer to the inclusive MC samples with (without) the signal processes. The pairs of pink solid (blue dashed) arrows indicate the signal (sideband) regions.

the 1-C kinematic fit is required to satisfy $0.90 < M_{\rm miss} < 0.98\,{\rm GeV}/c^2$. The distribution of $M_{\rm miss}$ before the 1-C kinematic fit is shown in figure 2(c).

By analyzing the $\psi(3686)$ inclusive MC samples with TopoAna [26], the only significant peaking background is found to be caused by the decays $\chi_{cJ} \to \Sigma^\pm\bar{\Lambda}\pi^\mp + {\rm c.c.}$ with $\Sigma^\pm \to n\pi^\pm$. The two pions in this decay may accidentally fall into the K^0_S mass window and fulfill the constraint for the secondary vertex fit, thus faking the K^0_S. This $\Sigma^\pm$ background peaks in the invariant mass spectrum of $nK^0_S\bar{\Lambda}$ (denoted as $M_{nK^0_S\bar{\Lambda}}$) but distributes uniformly in the $M_{\pi\pi}$ spectrum. Other backgrounds are smoothly distributed underneath the χ_{cJ} signals.

4 Branching fraction measurement

A simultaneous unbinned maximum-likelihood fit to the $M_{nK^0_S\bar{\Lambda}}$ spectra in both the $M_{\pi\pi}$ signal and sideband regions, as shown in figure 3, is performed to determine the signal yields and peaking backgrounds. The lower and upper sideband regions are defined as $[0.430, 0.466]$ and $[0.530, 0.566]\,{\rm GeV}/c^2$, respectively. The fit model for the signal region is

$$\sum_J (N_{1,J}\cdot f^J_{\rm signal} + N_{2,J}\cdot f^J_{\rm peakbkg}) + N_3\cdot f_{\rm flatbkg}\ (J=0,1,2)\,, \tag{4.1}$$

and that for the sideband region is

$$\sum_J (N'_{2,J}\cdot f^J_{\rm peakbkg}) + N'_3\cdot f'_{\rm flatbkg}\ (J=0,1,2)\,. \tag{4.2}$$

The signal shape $f^J_{\rm signal}$ for each χ_{cJ} resonance is described by its line shape convolved with a double-Gaussian function to account for the mass resolution. Each signal line shape is modeled with $BW(M_{nK^0_S\bar{\Lambda}})\times E^3_\gamma \times D(E_\gamma)$, where $BW(M_{nK^0_S\bar{\Lambda}}) = ((M_{nK^0_S\bar{\Lambda}} - m_{\chi_{cJ}})^2 + 0.25\Gamma^2_{\chi_{cJ}})^{-1}$ is the nonrelativistic Breit-Wigner function with the width $\Gamma_{\chi_{cJ}}$ and the mass $m_{\chi_{cJ}}$ of the corresponding χ_{cJ} fixed to the PDG values [13]; $E_\gamma = (m^2_{\psi(3686)} - M^2_{nK^0_S\bar{\Lambda}})/2m_{\psi(3686)}$ is the energy of the transition photon in the rest frame of $\psi(3686)$; $D(E_\gamma)$ is a damping factor that suppresses the divergent tail due to E^3_γ. This damping

JHEP11(2021)217

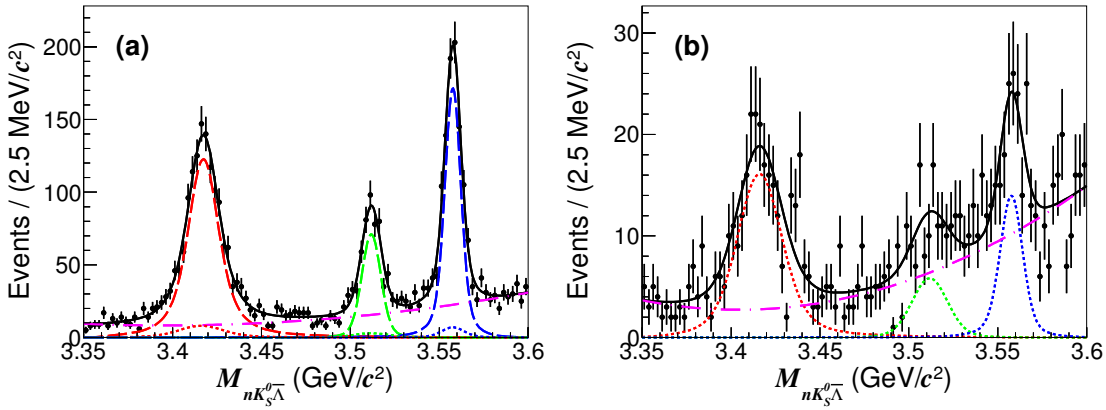

Figure 3. Simultaneous fit to the $M_{nK^0_S\bar{\Lambda}}$ spectra in the (a) signal and (b) sideband regions. The points with error bars are data. The black solid lines represent the total fit. The red, green, and blue dashed lines represent the signals of χ_{c0}, χ_{c1}, and χ_{c2}, respectively, and the corresponding dotted lines illustrate the peaking backgrounds. The purple dotted-dashed lines show the fitted backgrounds.

factor is described by $D(E_\gamma) = \exp(-E_\gamma^2/8\beta^2)$ with β constrainted to center value of the CLEO measurement (65.0 ± 2.5) MeV [27]. The uncertainty of β is considered as a source of systematic uncertainty. The two Gaussian functions in the convolution share the same mean value which is then floated in the fit. The relative width and size of the second Gaussian to the first Gaussian function are fixed to the results of MC studies, while the width of the first Gaussian function is floated. The peaking background shapes $f^J_{\rm peakbkg}$ are parameterized the same as the signal shapes. The yields $N_{2,J}$ in the signal region are normalized to $N'_{2,J}$ in the $M_{\pi\pi}$ sideband regions according to the sizes of these two regions. The background shapes $f^{(\prime)}_{\rm flatbkg}$ in both regions are modeled as second-order Chebyshev polynomial functions. The numbers of fitted χ_{cJ} signal events, $N_{1,J}$, are listed in table 1.

A special generator based on results of HelPWA [23–25] for the decay $\chi_{cJ} \to nK^0\bar{\Lambda} +$ c.c. is developed to estimate the detection efficiencies. The description of HelPWA can be found in the appendix A. For the χ_{cJ} data events used in HelPWA, the signal regions of $M_{nK^0_S\bar{\Lambda}}$ for χ_{c0}, χ_{c1}, and χ_{c2} are $[3.39, 3.45]$, $[3.50, 3.53]$, and $[3.54, 3.57]\,{\rm GeV}/c^2$, respectively; the masses of K^0, $\bar{\Lambda}$, and χ_{cJ} are constrained to their known masses [13]. The inclusive background MC sample is used to calculate the background likelihood with negative weight.

The signal MC events are generated with the HelPWA model, in which the parameters of coupling constants are determined by fitting the model to the χ_{cJ} data events. The Dalitz plots and the two-body invariant mass M_{ij} distributions of the data sample are shown in figures 4 and 5, respectively, where i and j denote the final state particles. The generated signal MC events based on HelPWA along with the simulated background events from the inclusive MC sample are represented as the solid lines in figure 5. The signal MC samples are generated with $\chi_{cJ} \to nK^0_S\bar{\Lambda}$ and $\chi_{cJ} \to \bar{n}K^0_S\Lambda$ separately. After applying the same event selection criteria to the signal MC samples, we fit the invariant mass spectra with the same methods used for the experimental data. The detection efficiencies of χ_{cJ},

JHEP11(2021)217

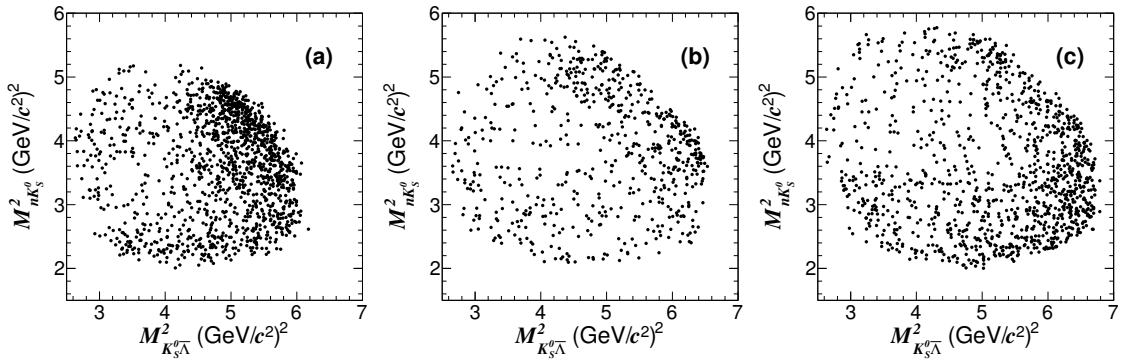

Figure 4. Dalitz plots of $M^2_{nK^0_S}$ versus $M^2_{K^0_S\bar{\Lambda}}$ for the (a) χ_{c0}, (b) χ_{c1}, and (c) χ_{c2} candidates in the data sample. The signal regions of $M_{nK^0_S\bar{\Lambda}}$ for χ_{c0}, χ_{c1}, and χ_{c2} are $[3.39, 3.45]$, $[3.50, 3.53]$, and $[3.54, 3.57]\,\mathrm{GeV}/c^2$, respectively.

Mode	$N_{1,J}$	ϵ_J (%)	BF (10^{-4})
χ_{c0}	1284 ± 50	9.95	$6.65 \pm 0.26 \pm 0.41$
χ_{c1}	399 ± 30	12.44	$1.66 \pm 0.12 \pm 0.12$
χ_{c2}	879 ± 40	13.03	$3.58 \pm 0.16 \pm 0.23$

Table 1. The number of fitted signal events ($N_{1,J}$), detection efficiency (ϵ_J), and $\mathcal{B}(\chi_{cJ} \to nK^0_S\bar{\Lambda}+$ c.c.), where the first uncertainty is statistical and the second one is systematic.

ϵ_J, are averaged over both charge conjugate channels and listed in table 1. The efficiency differences between the two charged conjugated modes are less than 0.5% for all three χ_{cJ} channels and are consistent within the statistical uncertainties.

The BFs are calculated using

$$\mathcal{B}(\chi_{cJ} \to nK^0_S\bar{\Lambda}) = \frac{N_{1,J}}{N_{\psi(3686)} \cdot \epsilon_J \cdot \prod_i \mathcal{B}_i}\,, \tag{4.3}$$

where $N_{\psi(3686)}$ is the number of $\psi(3686)$ events [12]; ϵ_J is the detection efficiency as listed in table 1; $\prod_i \mathcal{B}_i = \mathcal{B}(\psi(3686) \to \gamma\chi_{cJ}) \cdot \mathcal{B}(K^0_S \to \pi^+\pi^-) \cdot \mathcal{B}(\bar{\Lambda} \to \bar{p}\pi^+)$, where the BFs are taken from the PDG [13]. The results are summarized in table 1.

5 Systematic uncertainty

The number of $\psi(3686)$ events is measured to be $(4.48 \pm 0.03) \times 10^8$ based on inclusive hadronic events, as described in ref. [12], so the uncertainty is 0.6%. The systematic uncertainty due to the detection of γ is studied with the well understood channel $J/\psi \to \rho^0\pi^0$ [28]. The efficiency difference between data and MC simulation is about 1% per photon. To estimate the uncertainties associated with K^0_S and Λ reconstruction, the decays $J/\psi \to K^{*\pm}(892)K^{\mp}$, $K^{*\pm}(892) \to K^0_S\pi^{\pm}$ and $J/\psi \to \Lambda\bar{\Lambda}$ are selected as the control samples. The uncertainties are determined to be 1.5% per K^0_S and 2.0% per Λ. The systematic uncertainty caused by the 1-C kinematic fit is studied with the control sample

JHEP11(2021)217

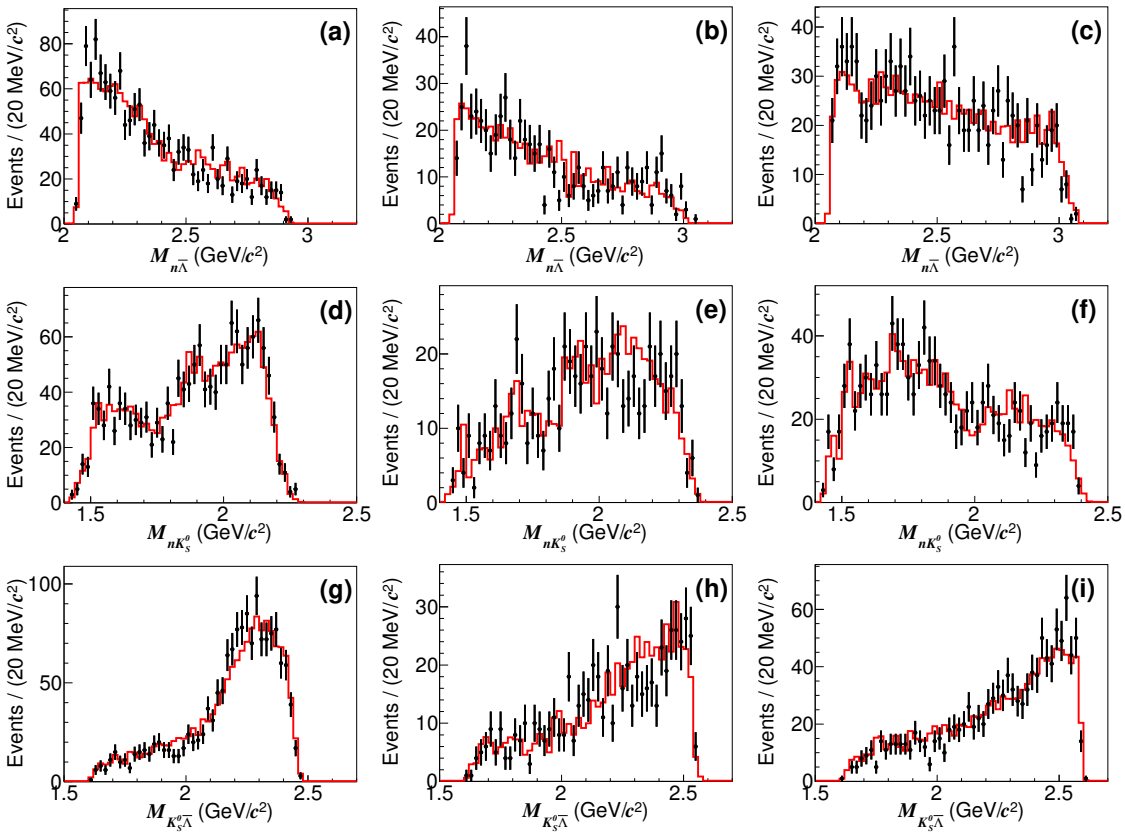

Figure 5. Distributions of $M_{n\bar{\Lambda}}$, $M_{nK_S^0}$, and $M_{K_S^0\bar{\Lambda}}$ for $\chi_{cJ} \to nK_S^0\bar{\Lambda}+$c.c. ($J = 0,\ 1,\ 2$). The left column is for χ_{c0}, the middle column is for χ_{c1}, and the right column is for χ_{c2}. The data are represented by black points with error bars and the MC events are represented by red lines. The signal regions of $M_{nK_S^0\bar{\Lambda}}$ for χ_{c0}, χ_{c1}, and χ_{c2} are $[3.39, 3.45]$, $[3.50, 3.53]$, and $[3.54, 3.57]\,\mathrm{GeV}/c^2$, respectively.

$\psi(3686) \to \pi^0 nK_S^0\bar{\Lambda}$ with purity about 98.5%, where n, K_S^0, and $\bar{\Lambda}$ are selected using the same criteria as the nominal analysis but the number of good photons is required to be at least two. The difference of the selection efficiencies between data and MC simulation is determined to be 4.1% and assigned as the corresponding systematic uncertainty. The uncertainties associated with the mass windows of K_S^0, Λ, and $M_{\rm miss}$ are estimated by repeating the analysis with alternative mass window requirements. We change the mass window of K_S^0 to $[0.473, 0.521]$ and $[0.487, 0.511]\,\mathrm{GeV}/c^2$, that of Λ to $[1.110, 1.123]$ and $[1.113, 1.119]\,\mathrm{GeV}/c^2$, and that of $M_{\rm miss}$ to [0.880, 1.000] and [0.910, 0.970] GeV/c^2. The largest differences from the nominal BFs are assigned as the corresponding systematic uncertainties.

The systematic uncertainty related to the fitting procedure includes multiple sources. For the signal line shape, the parameterization of the damping factor may introduce a systematic uncertainty. The nominal damping factor is changed to another popular form used by KEDR [29], given by $D(E_\gamma) = \frac{E_{\gamma 0}^2}{E_\gamma E_{\gamma 0}+(E_\gamma - E_{\gamma 0})^2}$, where $E_{\gamma 0} = (m_{\psi(3686)}^2 - M_{\chi_{cJ}}^2)/2m_{\psi(3686)}$. The resulting differences in the fit are assigned as the related systematic

JHEP11(2021)217

Sources	$\mathcal{B}(\chi_{c0})$	$\mathcal{B}(\chi_{c1})$	$\mathcal{B}(\chi_{c2})$
$N_{\psi(3686)}$	0.6	0.6	0.6
γ detection	1.0	1.0	1.0
K_S^0 reconstruction	1.5	1.5	1.5
Λ reconstruction	2.0	2.0	2.0
Kinematic fit	4.1	4.1	4.1
Mass windows	0.4	0.7	0.5
Fitting procedure	2.8	4.1	2.3
MC modeling	1.3	1.3	2.3
Input BFs	2.2	2.6	2.2
Total	6.2	7.1	6.3

Table 2. Systematic uncertainty sources and their contributions (in %).

uncertainties. In addition, the background function is changed from a second to a third order Chebyshev function, and the differences in signal yields are taken as the systematic uncertainties. The systematic uncertainty due to the fit range is evaluated by changing the fit range from $[3.35, 3.60]$ to $[3.35, 3.65]$ and $[3.30, 3.65]\,\mathrm{GeV}/c^2$, and the maximum differences in the fitted yields are considered as the associated systematic uncertainties. The total uncertainties of the fitting procedure are estimated to be 2.8%, 4.1%, and 2.3% for χ_{c0}, χ_{c1}, and χ_{c2}, respectively.

The systematic uncertainties arising from MC modeling are estimated by using different model parameters and taking into account contribution from intermediate resonances with small significance in HelPWA. The differences of efficiencies based on the new HelPWA results and the nominal ones are taken as the uncertainties. The systematic uncertainties due to the input BFs of $\psi(3686) \to \gamma\chi_{c0}$ (χ_{c1}, χ_{c2}), $K_S^0 \to \pi^+\pi^-$, and $\Lambda \to p\pi^-$ are 2.0% (2.5%, 2.1%), 0.1%, and 0.8%, respectively, according to the PDG [13].

All systematic uncertainty contributions are summarized in table 2. The total systematic uncertainty for each χ_{cJ} decay is obtained by adding all contributions in quadrature.

6 Summary

The decays of $\chi_{cJ} \to nK_S^0\bar{\Lambda}+\text{c.c.}$ ($J = 0, 1, 2$) are observed for the first time using $(4.48 \pm 0.03) \times 10^8$ $\psi(3686)$ events accumulated with the BESIII detector at the BEPCII collider. The BFs of $\chi_{cJ} \to nK_S^0\bar{\Lambda}$ + c.c. are determined to be $(6.65 \pm 0.26_{\text{stat}} \pm 0.41_{\text{syst}}) \times 10^{-4}$, $(1.66 \pm 0.12_{\text{stat}} \pm 0.12_{\text{syst}}) \times 10^{-4}$, and $(3.58 \pm 0.16_{\text{stat}} \pm 0.23_{\text{syst}}) \times 10^{-4}$ for $J = 0$, 1, and 2, respectively. Isospin symmetry is examined by comparing our results with the isospin conjugate decays of $\chi_{cJ} \to pK^-\bar{\Lambda} + \text{c.c.}$ [11]. The ratios $\mathcal{B}(\chi_{cJ} \to pK^-\bar{\Lambda} + \text{c.c.})/\mathcal{B}(\chi_{cJ} \to nK_S^0\bar{\Lambda}+\text{c.c.})$ are measured to be $1.98\pm0.09_{\text{stat}}\pm0.14_{\text{syst}}$, $2.71\pm0.24_{\text{stat}}\pm0.20_{\text{syst}}$, and $2.35\pm 0.14_{\text{stat}} \pm 0.16_{\text{syst}}$ for $J = 0$, 1, and 2, respectively, where common sources of systematic uncertainties are canceled. No obvious isospin violation is observed.

JHEP11(2021)217

Enhancements are observed in the Dalitz plots shown in figure 4 and the mass distributions of two-body $n\bar{\Lambda}$ subsystems shown in figure 5. We perform a HelPWA with the main goal to produce MC samples that describe the data well enough to obtain a good estimate of the efficiency. While the HelPWA does describe the data nicely, the complexity of the model we used here does not allow to draw any firm conclusions on the relative contributions of individual resonances.

Acknowledgments

The BESIII collaboration thanks the staff of BEPCII and the IHEP computing center for their strong support. This work is supported in part by National Key Research and Development Program of China under Contracts Nos. 2020YFA0406300, 2020YFA0406400; National Natural Science Foundation of China (NSFC) under Contracts Nos. 11875170, 11875115, 11475090, 11625523, 11635010, 11735014, 11822506, 11835012, 11875054, 11875262, 11935015, 11935016, 11935018, 11961141012, 12022510, 12035009, 12035013, 12061131003; the Chinese Academy of Sciences (CAS) Large-Scale Scientific Facility Program; Joint Large-Scale Scientific Facility Funds of the NSFC and CAS under Contracts Nos. U2032110, U2032104, U1732263, U1832207; CAS Key Research Program of Frontier Sciences under Contract No. QYZDJ-SSW-SLH040; 100 Talents Program of CAS; INPAC and Shanghai Key Laboratory for Particle Physics and Cosmology; ERC under Contract No. 758462; European Union Horizon 2020 research and innovation programme under Contract No. Marie Sklodowska-Curie grant agreement No 894790; German Research Foundation DFG under Contracts No. 443159800, Collaborative Research Center CRC 1044, FOR 2359, FOR 2359, GRK 214; Istituto Nazionale di Fisica Nucleare, Italy; Ministry of Development of Turkey under Contract No. DPT2006K-120470; National Science and Technology fund; Olle Engkvist Foundation under Contract No. 200-0605; STFC (U.K.); The Knut and Alice Wallenberg Foundation (Sweden) under Contract No. 2016.0157; The Royal Society, U.K. under Contracts No. DH140054, DH160214; The Swedish Research Council; U. S. Department of Energy under Contracts Nos. DE-FG02-05ER41374, DE-SC-0012069.

A HelPWA model

A.1 Variable definition

Four-momentum vectors of final states for the decay $\chi_{cJ} \to nK_S^0\bar{\Lambda}$ are denoted by p_1, p_2 and p_3. Momentum combinations, $p_i + p_j$ and $p_i + p_j + p_k$, are denoted by $[ij]$ and $[ijk]$, respectively. The production of $nK_S^0\bar{\Lambda}$ events, as shown in figure 6, is assumed via intermediate states Λ^*, K^*, N^* and direct three-body decay,

$$(a): \quad \chi_{cJ} \to \Lambda^*\bar{\Lambda}, \qquad \Lambda^* \to nK_S^0, \tag{A.1}$$

$$(b): \quad \chi_{cJ} \to K_S^0 K^{*+}, \quad K^{*+} \to n\bar{\Lambda}, \tag{A.2}$$

$$(c): \quad \chi_{cJ} \to n\bar{N}^*, \qquad \bar{N}^* \to K_S^0\bar{\Lambda}. \tag{A.3}$$

$$(d): \quad \chi_{cJ} \to nK_S^0\bar{\Lambda}. \tag{A.4}$$

JHEP11(2021)217

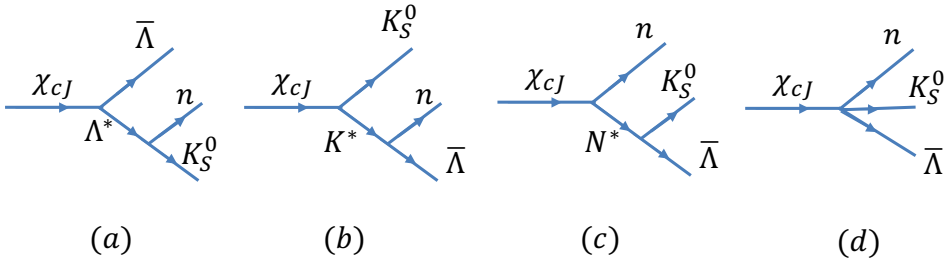

Figure 6. The quasi-two body decays and the direct three-body decays in the process $\chi_{cJ} \to nK_S^0\bar{\Lambda}$.

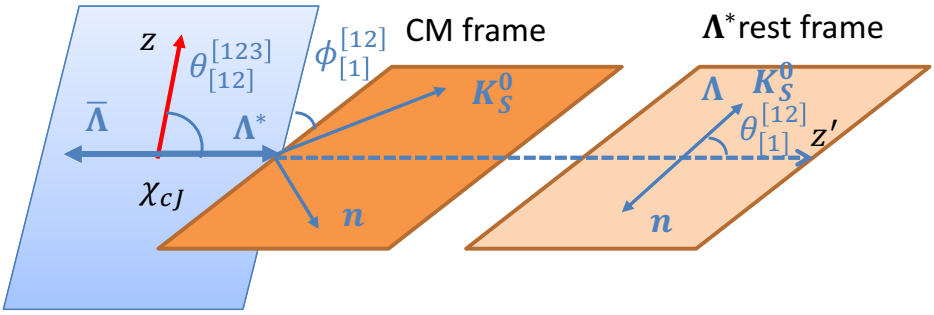

Figure 7. Helicity system of the decay $\chi_{cJ} \to \Lambda^*\bar{\Lambda}$, $\Lambda^* \to nK_S^0$.

For the decay $\chi_{cJ} \to A(p_A)B(p_B)$, the helicity angles are taken as the polar and azimuthal angles for the momentum $\mathbf{p}_A$ in the χ_{cJ} rest frame. Let $\hat{x}$, $\hat{y}$ and $\hat{z}$ be the coordinate system fixed in the χ_{cJ} rest frame. For the second decay, $A \to X(p_X)Y(p_Y)$, the z axis, $\hat{z}_h$, is taken along the flying direction of the A in the χ_{cJ} rest frame, and momenta p_X and p_Y are defined in the A rest frame. Then the helicity coordinate system fixed by the A decay is defined as $\hat{y}_h \propto \hat{z} \times \hat{z}_h$ and $\hat{x}_h = \hat{y}_h \times \hat{z}_h$. The helicity angles for the second decay are taken as the polar and azimuthal angles for the momentum $\mathbf{p}_X$ in the helicity system $(\hat{x}_h, \hat{y}_h, \hat{z}_h)$. Figure 7 shows the helicity system definition for type (a) decay, for example. Variable definitions for the helicity angles and amplitudes are given in table 3 for the sequential decays (a), (b) and (c).

A.2 Decay amplitude

Decay amplitude for process (a) reads

$$A_1(m,\lambda_1,\lambda_3) = \sum_{\lambda_R} F^{\chi_{cJ}}_{\lambda_R,\lambda_3} D^{J*}_{m,\lambda_R-\lambda_3}(\phi^{[123]}_{[12]},\theta^{[123]}_{[12]},0) BW(m_{12}) F^{\Lambda^*}_{\lambda_1,0} D^{J_R*}_{\lambda_R,\lambda_1}(\phi^{[12]}_{[1]},\theta^{[12]}_{[1]},0), \tag{A.5}$$

where $D^J_{m,\lambda}(\phi,\theta,0)$ is Wigner-D function with $J = 0,1,2$ for χ_{cJ} states, J_R is the spin of resonance Λ^*, and BW denotes Breit-Wigner function.

Decay amplitude for the process (b) reads

$$\begin{aligned} A_2(m,\lambda_1,\lambda_3) = \sum_{\lambda_+,\lambda_1',\lambda_3'} & F^{\chi_{cJ}}_{\lambda_+,0} D^{J*}_{m,\lambda_+}(\phi^{[123]}_{[13]},\theta^{[123]}_{[13]},0) BW(m_{13}) F^{K^{*+}}_{\lambda_3',\lambda_1'} D^{J_R*}_{\lambda_+,\lambda_3'-\lambda_1'}(\phi^{[13]}_{[3]},\theta^{[13]}_{[3]},0) \\ & \times D^{\frac{1}{2}}_{\lambda_3',\lambda_3}(\phi_2',\theta_2',\psi_2') D^{\frac{1}{2}}_{\lambda_1',\lambda_1}(\phi_3',\theta_3',\psi_3'), \end{aligned} \tag{A.6}$$

JHEP11(2021)217

Decays	Helicity angles	Helicity amplitudes
$\chi_{cJ}(m) \to \Lambda^*(\lambda_R)\bar{\Lambda}(\lambda_3)$	$\theta^{[123]}_{[12]}, \phi^{[123]}_{[12]}$	$F^{\chi_{cJ}}_{\lambda_R,\lambda_3}$
$\Lambda^* \to n(\lambda_1)K^0_S$	$\theta^{[12]}_{[1]}, \phi^{[12]}_{[1]}$	$F^{\Lambda^*}_{\lambda_1,0}$
$\chi_{cJ}(m) \to K^{*+}(\lambda_+)K^0_S$	$\theta^{[123]}_{[13]}, \phi^{[123]}_{[13]}$	$F^{\chi_{cJ}}_{\lambda_+,0}$
$K^{*+} \to \bar{\Lambda}(\lambda_3)n(\lambda_1)$	$\theta^{[13]}_{[3]}, \phi^{[13]}_{[3]}$	$F^{K^{*+}}_{\lambda_3,\lambda_1}$
$\chi_{cJ}(m) \to \bar{N}^{*-}(\lambda_-)n(\lambda_1)$	$\theta^{[123]}_{[23]}, \phi^{[123]}_{[23]}$	$F^{\chi_{cJ}}_{\lambda_-,\lambda_1}$
$\bar{N}^{*-} \to \bar{\Lambda}(\lambda_3)K^0_S$	$\theta^{[23]}_{[3]}, \phi^{[23]}_{[3]}$	$F^{\bar{N}^{*-}}_{\lambda_3,0}$

Table 3. Helicity angles and amplitudes of the sequential decays (a), (b) and (c). λ_i denotes the value of helicity for the corresponding particle, and m denotes the spin z projection of virtual photon χ_{cJ}.

where J_R is the spin of K^{*+}. The angles $(\phi'_2, \theta'_2, \psi'_2)$ and $(\phi'_3, \theta'_3, \psi'_3)$ correspond to the rotation to align the $\bar{\Lambda}$ and n helicity system to coincide with those defined in the process (a). These rotations carry the polarization of Λ and n into the helicity system of (a), so that ensures the coherent interference between the two decays. This issue has been addressed in the analyses [30, 31] and proved in ref. [32].

Decay amplitude for process (c) reads

$$A_3(m,\lambda_1,\lambda_3) = \sum_{\lambda_-,\lambda'_1,\lambda'_3} F^{\chi_{cJ}}_{\lambda_-,\lambda'_1} D^{J*}_{m,\lambda_- -\lambda'_1}(\phi^{[123]}_{[23]}, \theta^{[123]}_{[23]}, 0) BW(m_{23}) F^{\bar{N}^{*-}}_{\lambda'_3,0} D^{J_R*}_{\lambda_-,\lambda'_3}(\phi^{[23]}_{[3]}, \theta^{[23]}_{[3]}, 0) \times D^{\frac{1}{2}}_{\lambda'_3,\lambda_3}(\phi'_2, \theta'_2, \psi'_2) D^{\frac{1}{2}}_{\lambda'_1,\lambda_1}(\phi'_3, \theta'_3, \psi'_3), \tag{A.7}$$

where the two factors $D^{\frac{1}{2}}_{\lambda'_3,\lambda_3}(\phi'_2, \theta'_2, \psi'_2)$ and $D^{\frac{1}{2}}_{\lambda'_1,\lambda_1}(\phi'_3, \theta'_3, \psi'_3)$ correspond to the rotation of $\bar{\Lambda}$ and neutron helicities to coincide with those defined in the process (a).

Helicity amplitude is expressed with partial waves in terms of LS-coupling scheme [23, 33, 34]. For two-body decays with spin $J \to s + \sigma$, it follows

$$F^J_{\lambda,\nu} = \sum_{ls} \left(\frac{2l+1}{2J+1}\right)^{1/2} \langle l0S\delta|J\delta\rangle \langle s\lambda\sigma - \nu|S\delta\rangle g_{lS} r^l \frac{B_l(r)}{B_l(r_0)}, \tag{A.8}$$

where L and S are the orbital angular momentum and spin quantum numbers for the two-body decay, r is the magnitude of the relative momentum of the final states, r_0 is the corresponding momentum at the R nominal mass, g_{ls} is a coupling constant to be determined, and $B_L(r)$ is the Blatt-Weisskopf barrier factor [24].

The non-resonant decay is described with the helicity amplitude constructed in the event system, in which the X–Y plane is chosen as the three-body decay plane, and the Z-axis is defined as the normal to the decay plane. To describe the n, K^0_S and Λ orientations in the X–Y–Z system, one needs to introduce three rotations to carry the momenta of

JHEP11(2021)217

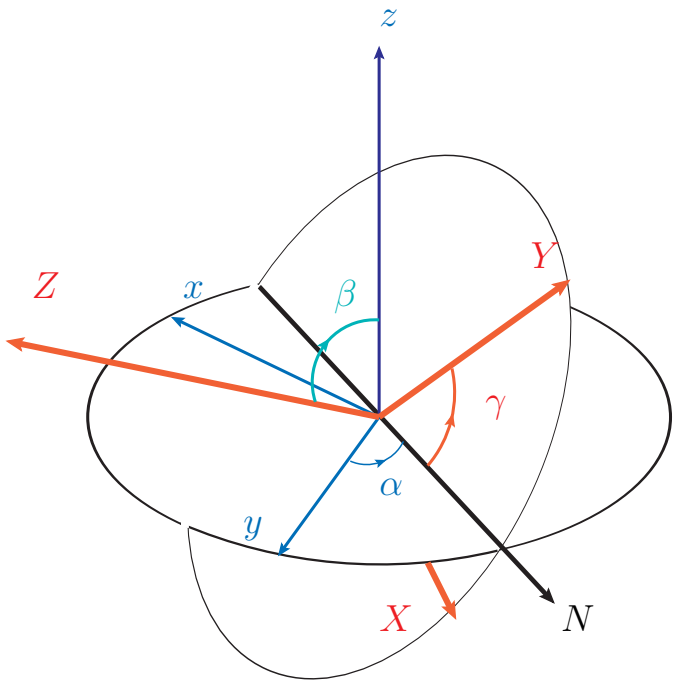

Figure 8. Illustration of rotations to carry the n, K_S^0 and Λ orientations from the χ_{cJ} rest frame xyz to the three body helicity system XYZ by the three Euler angles α, β and γ.

final states from the χ_{cJ} rest frame, x–y–z to the three-body helicity system, X–Y–Z by three Euler angles, α, β,and γ as shown in figure 8. The calculations of Euler angles can be found in [35].

The amplitude is written as [25],

$$B_m = \sum_{\mu} D^{J*}_{m,\mu}(\alpha, \beta, \gamma) T_{\lambda_1,\lambda_2,\lambda_3} \,, \tag{A.9}$$

where m denotes the z-component of the χ_{cJ} spin in its rest frame. The decay amplitude $T_{\lambda_1,\lambda_2,\lambda_3}$ is a fit constant depending on the helicity values λ_i of the final state particles, and μ is the helicity of the χ_{cJ} in the helicity system fixed to the three-body reference, which is summed over.

A.3 Fit method

To determine the decay coupling constants g_{ls} and decay amplitude T, we fit the model to the data events by minimizing the function defined as

$$S = -(\ln \mathcal{L}_{\rm data} - \ln \mathcal{L}_{\rm bg}), \tag{A.10}$$

where the contributions from background events are subtracted from the likelihood of observed data events $\mathcal{L}_{\rm data}$, and the likelihood function $\mathcal{L}$ for the N data events is defined with the amplitudes as

$$\mathcal{L} = \prod_{j=1}^{N} \sum_{m,\lambda_1,\lambda_3} \frac{\rho^J_{m,m}}{\sigma_{\rm MC}} \left| \sum_i A_i(m, \lambda_1, \lambda_3) + B_m \right|^2_j , \tag{A.11}$$

JHEP11(2021)217

where ρ^J is the spin density matrix for the χ_{cJ} production from the $\psi(3686) \to \gamma\chi_{cJ}$ decay, and they are taken as $\rho^0 = 1$, $\rho^1 = \frac{1}{4}\begin{pmatrix} 1 & 0 & 0 \\ 0 & 2 & 0 \\ 0 & 0 & 1 \end{pmatrix}$ and $\rho^2 = \frac{3}{20}\begin{pmatrix} 2 & 0 & 0 & 0 & 0 \\ 0 & 1 & 0 & 0 & 0 \\ 0 & 0 & 2/3 & 0 & 0 \\ 0 & 0 & 0 & 1 & 0 \\ 0 & 0 & 0 & 0 & 2 \end{pmatrix}$ [32] for χ_{c0}, χ_{c1} and χ_{c2}, respectively. The amplitude summation $\sum_i A_i(\dots)$ is taken over all intermediate states, and $|\dots|_j$ denotes the amplitude calculated with the angular observables of j-th event. The normalization factor $\sigma_{\rm MC}$ is calculated as the average of amplitudes with a sample of simulated MC phase space events.

To describe the data distributions with the model, we use the 16 intermediate states [excited Λ: $\Lambda(1405)$, $\Lambda(1520)$, $\Lambda(1600)$, $\Lambda(1670)$, $\Lambda(1690)$, $\Lambda(1800)$, $\Lambda(1890)$, $\Lambda(2000)$, $\Lambda(2020)$, $\Lambda(2100)$, $\Lambda(2110)$, $\Lambda(2325)$, $\Lambda(2350)$; excited N: $N^*(2300)$; excited K: $K_2(2250)$], and the non-resonant decay. The masses and widths of these states are fixed to the PDG values [13] in the fit. The possible interferences between the non-resonant process and the processes with intermediate states are also included, and parity conservation is required to reduce the number of independent helicity amplitudes.

References

[1] S.M.H. Wong, *Color octet contribution in exclusive p wave charmonium decay into octet and decuplet baryons*, *Eur. Phys. J. C* **14** (2000) 643 [hep-ph/9903236] [INSPIRE].

[2] BESIII collaboration, *Spin-Parity Analysis of $p\bar{p}$ Mass Threshold Structure in J/ψ and ψ' Radiative Decays*, *Phys. Rev. Lett.* **108** (2012) 112003 [arXiv:1112.0942] [INSPIRE].

[3] BES collaboration, *Observation of a threshold enhancement in the $p\overline{\Lambda}$ invariant mass spectrum*, *Phys. Rev. Lett.* **93** (2004) 112002 [hep-ex/0405050] [INSPIRE].

[4] A. Datta and P.J. O'Donnell, *A New state of baryonium*, *Phys. Lett. B* **567** (2003) 273 [hep-ph/0306097] [INSPIRE].

[5] B. Loiseau and S. Wycech, *Antiproton-proton channels in J/ψ decays*, *Phys. Rev. C* **72** (2005) 011001 [hep-ph/0501112] [INSPIRE].

[6] M.-L. Yan, S. Li, B. Wu and B.-Q. Ma, *Nucleon-antinucleon bound states in Skyrmion-type potential*, *Phys. Rev. D* **72** (2005) 034027 [hep-ph/0405087] [INSPIRE].

[7] B. Kerbikov, A. Stavinsky and V. Fedotov, *Model independent view on the low mass proton anti-proton enhancement*, *Phys. Rev. C* **69** (2004) 055205 [hep-ph/0402054] [INSPIRE].

[8] J. Haidenbauer, U.-G. Meißner and A. Sibirtsev, *Near threshold $p\bar{p}$ enhancement in B and J/ψ decay*, *Phys. Rev. D* **74** (2006) 017501 [hep-ph/0605127] [INSPIRE].

[9] D.R. Entem and F. Fernández, *Final state interaction effects in near threshold enhancement of the $p\bar{p}$ mass spectrum in B and J/ψ decays*, *Phys. Rev. D* **75** (2007) 014004 [INSPIRE].

[10] BES collaboration, *First observation of J/ψ and $\psi(2S)$ decaying to $nK^0_S\bar{\Lambda} + c.c.$*, *Phys. Lett. B* **659** (2008) 789 [arXiv:0710.3091] [INSPIRE].

[11] BESIII collaboration, *Measurements of $\psi' \to \bar{p}K^+\Sigma^0$ and $\chi_{cJ} \to \bar{p}K^+\Lambda$*, *Phys. Rev. D* **87** (2013) 012007 [arXiv:1211.5631] [INSPIRE].

JHEP11(2021)217

[12] BESIII collaboration, *Determination of the number of $\psi(3686)$ events at BESIII*, *Chin. Phys. C* **42** (2018) 023001 [arXiv:1709.03653] [INSPIRE].

[13] PARTICLE DATA collaboration, *Review of Particle Physics*, *Prog. Theor. Exp. Phys.* **2020** (2020) 083C01 [INSPIRE].

[14] BESIII collaboration, *Design and Construction of the BESIII Detector*, *Nucl. Instrum. Meth. A* **614** (2010) 345 [arXiv:0911.4960] [INSPIRE].

[15] BESIII collaboration, *Future Physics Programme of BESIII*, *Chin. Phys. C* **44** (2020) 040001 [arXiv:1912.05983] [INSPIRE].

[16] C. Yu et al., *BEPCII Performance and Beam Dynamics Studies on Luminosity*, in proceedings of the *International Particle Accelerator Conference (IPAC'16)*, Busan, Korea, 8–13 May 2016, in *International Particle Accelerator Conference* **7**, JACoW, Geneva Switzerland (2016), pp. 1014–1018.

[17] GEANT4 collaboration, *GEANT4 — a simulation toolkit*, *Nucl. Instrum. Meth. A* **506** (2003) 250 [INSPIRE].

[18] S. Jadach, B.F.L. Ward and Z. Wąs, *Coherent exclusive exponentiation for precision Monte Carlo calculations*, *Phys. Rev. D* **63** (2001) 113009 [hep-ph/0006359] [INSPIRE].

[19] D.J. Lange, *The EvtGen particle decay simulation package*, *Nucl. Instrum. Meth. A* **462** (2001) 152 [INSPIRE].

[20] J.C. Chen, G.S. Huang, X.R. Qi, D.H. Zhang and Y.S. Zhu, *Event generator for J/ψ and $\psi(2S)$ decay*, *Phys. Rev. D* **62** (2000) 034003 [INSPIRE].

[21] E. Richter-Was, *QED bremsstrahlung in semileptonic B and leptonic tau decays*, *Phys. Lett. B* **303** (1993) 163 [INSPIRE].

[22] BESIII collaboration, *Measurement of higher-order multipole amplitudes in $\psi(3686) \to \gamma\chi_{c1,2}$ with $\chi_{c1,2} \to \gamma J/\psi$ and search for the transition $\eta_c(2S) \to \gamma J/\psi$*, *Phys. Rev. D* **95** (2017) 072004 [arXiv:1701.01197] [INSPIRE].

[23] S.U. Chung, *A General formulation of covariant helicity coupling amplitudes*, *Phys. Rev. D* **57** (1998) 431 [INSPIRE].

[24] B.S. Zou and D.V. Bugg, *Covariant tensor formalism for partial-wave analyses of ψ decay to mesons*, *Eur. Phys.* **16** (2003) 537.

[25] S.M. Berman and M. Jacob, *Systematics of angular polarization distributions in three-body decays*, *Phys. Rev.* **139** (1965) B1023 [INSPIRE].

[26] X. Zhou, S. Du, G. Li and C. Shen, *TopoAna: A generic tool for the event type analysis of inclusive Monte-Carlo samples in high energy physics experiments*, *Comput. Phys. Commun.* **258** (2021) 107540.

[27] CLEO collaboration, *J/ψ and $\psi(2S)$ Radiative Transitions to η_c*, *Phys. Rev. Lett.* **102** (2009) 011801 [*Erratum ibid.* **106** (2011) 159903] [arXiv:0805.0252] [INSPIRE].

[28] BESIII collaboration, *Measurement of χ_{cJ} decaying into $p\bar{n}\pi^-$ and $p\bar{n}\pi^-\pi^0$*, *Phys. Rev. D* **86** (2012) 052011 [arXiv:1208.3721] [INSPIRE].

[29] V.M. Anashin et al., *Measurement of $\mathcal{B}(J/\psi \to \eta_c\gamma)$ at KEDR*, *Int. J. Mod. Phys. Conf. Ser.* **2** (2011) 188 [arXiv:1012.1694] [INSPIRE].

[30] LHCb collaboration, *Observation of $J/\psi p$ Resonances Consistent with Pentaquark States in $\Lambda_b^0 \to J/\psi K^- p$ Decays*, *Phys. Rev. Lett.* **115** (2015) 072001 [arXiv:1507.03414] [INSPIRE].

JHEP11(2021)217

[31] Belle collaboration, *Experimental constraints on the spin and parity of the $Z(4430)^+$*, *Phys. Rev. D* **88** (2013) 074026 [arXiv:1306.4894] [INSPIRE].

[32] H. Chen and R.-G. Ping, *Coherent helicity amplitude for sequential decays*, *Phys. Rev. D* **95** (2017) 076010 [arXiv:1704.05184] [INSPIRE].

[33] S.U. Chung, *Helicity coupling amplitudes in tensor formalism*, *Phys. Rev. D* **48** (1993) 1225 [*Erratum ibid.* **56** (1997) 4419] [INSPIRE].

[34] S.U. Chung and J.M. Friedrich, *Covariant helicity-coupling amplitudes: A New formulation*, *Phys. Rev. D* **78** (2008) 074027 [arXiv:0711.3143] [INSPIRE].

[35] V. Devanathan, *Angular Momentum Techniques in Quantum Mechanics*, Kluwer Academic Publishers (2002).

JHEP11(2021)217

The BESIII collaboration

M. Ablikim,[1] M.N. Achasov,[10,b] P. Adlarson,[67] S. Ahmed,[15] M. Albrecht,[4] R. Aliberti,[28] A. Amoroso,[66A,66C] M.R. An,[32] Q. An,[63,49] X.H. Bai,[57] Y. Bai,[48] O. Bakina,[29] R. Baldini Ferroli,[23A] I. Balossino,[24A] Y. Ban,[38,h] K. Begzsuren,[26] N. Berger,[28] M. Bertani,[23A] D. Bettoni,[24A] F. Bianchi,[66A,66C] J. Bloms,[60] A. Bortone,[66A,66C] I. Boyko,[29] R.A. Briere,[5] H. Cai,[68] X. Cai,[1,49] A. Calcaterra,[23A] G.F. Cao,[1,54] N. Cao,[1,54] S.A. Cetin,[53A] J.F. Chang,[1,49] W.L. Chang,[1,54] G. Chelkov,[29,a] D.Y. Chen,[6] G. Chen,[1] H.S. Chen,[1,54] M.L. Chen,[1,49] S.J. Chen,[35] X.R. Chen,[25] Y.B. Chen,[1,49] Z.J. Chen,[20,i] W.S. Cheng,[66C] G. Cibinetto,[24A] F. Cossio,[66C] X.F. Cui,[36] H.L. Dai,[1,49] J.P. Dai,[42,e] X.C. Dai,[1,54] A. Dbeyssi,[15] R. E. de Boer,[4] D. Dedovich,[29] Z.Y. Deng,[1] A. Denig,[28] I. Denysenko,[29] M. Destefanis,[66A,66C] F. De Mori,[66A,66C] Y. Ding,[33] C. Dong,[36] J. Dong,[1,49] L.Y. Dong,[1,54] M.Y. Dong,[1,49,54] X. Dong,[68] S.X. Du,[71] Y.L. Fan,[68] J. Fang,[1,49] S.S. Fang,[1,54] Y. Fang,[1] R. Farinelli,[24A] L. Fava,[66B,66C] F. Feldbauer,[4] G. Felici,[23A] C.Q. Feng,[63,49] J.H. Feng,[50] M. Fritsch,[4] C.D. Fu,[1] Y. Gao,[38,h] Y. Gao,[64] Y. Gao,[63,49] Y.G. Gao,[6] I. Garzia,[24A,24B] P.T. Ge,[68] C. Geng,[50] E.M. Gersabeck,[58] A. Gilman,[61] K. Goetzen,[11] L. Gong,[33] W.X. Gong,[1,49] W. Gradl,[28] M. Greco,[66A,66C] L.M. Gu,[35] M.H. Gu,[1,49] Y.T. Gu,[13] C.Y. Guan,[1,54] A.Q. Guo,[22] L.B. Guo,[34] R.P. Guo,[40] Y.P. Guo,[9,f] A. Guskov,[29,a] T.T. Han,[41] W.Y. Han,[32] X.Q. Hao,[16] F.A. Harris,[56] K.L. He,[1,54] F.H. Heinsius,[4] C.H. Heinz,[28] Y.K. Heng,[1,49,54] C. Herold,[51] M. Himmelreich,[11,d] T. Holtmann,[4] G.Y. Hou,[1,54] Y.R. Hou,[54] Z.L. Hou,[1] H.M. Hu,[1,54] J.F. Hu,[47,j] T. Hu,[1,49,54] Y. Hu,[1] G.S. Huang,[63,49] L.Q. Huang,[64] X.T. Huang,[41] Y.P. Huang,[1] Z. Huang,[38,h] T. Hussain,[65] N. Hüsken,[22,28] W. Ikegami Andersson,[67] W. Imoehl,[22] M. Irshad,[63,49] S. Jaeger,[4] S. Janchiv,[26] Q. Ji,[1] Q.P. Ji,[16] X.B. Ji,[1,54] X.L. Ji,[1,49] Y.Y. Ji,[41] H.B. Jiang,[41] X.S. Jiang,[1,49,54] J.B. Jiao,[41] Z. Jiao,[18] S. Jin,[35] Y. Jin,[57] M.Q. Jing,[1,54] T. Johansson,[67] N. Kalantar-Nayestanaki,[55] X.S. Kang,[33] R. Kappert,[55] M. Kavatsyuk,[55] B.C. Ke,[71] I.K. Keshk,[4] A. Khoukaz,[60] P. Kiese,[28] R. Kiuchi,[1] R. Kliemt,[11] L. Koch,[30] O.B. Kolcu,[53A] B. Kopf,[4] M. Kuemmel,[4] M. Kuessner,[4] A. Kupsc,[67] M.G. Kurth,[1,54] W. Kühn,[30] J.J. Lane,[58] J.S. Lange,[30] P. Larin,[15] A. Lavania,[21] L. Lavezzi,[66A,66C] Z.H. Lei,[63,49] H. Leithoff,[28] M. Lellmann,[28] T. Lenz,[28] C. Li,[39] C.H. Li,[32] C. Li,[63,49] D.M. Li,[71] F. Li,[1,49] G. Li,[1] H. Li,[43] H. Li,[63,49] H.B. Li,[1,54] H.J. Li,[16] J.L. Li,[41] J.Q. Li,[4] J.S. Li,[50] K. Li,[1] L.K. Li,[1] L. Li,[3] P.R. Li,[31,k,l] S.Y. Li,[52] W.D. Li,[1,54] W.G. Li,[1] X.H. Li,[63,49] X.L. Li,[41] X. Li,[1,54] Z.Y. Li,[50] H. Liang,[63,49] H. Liang,[1,54] H. Liang,[27] Y.F. Liang,[45] Y.T. Liang,[25] G.R. Liao,[12] L.Z. Liao,[1,54] J. Libby,[21] A. Limphirat,[51] C.X. Lin,[50] B.J. Liu,[1] C.X. Liu,[1] D. Liu,[15,63] F.H. Liu,[44] F. Liu,[1] F. Liu,[6] H.B. Liu,[13] H.M. Liu,[1,54] H. Liu,[1] H. Liu,[17] J.B. Liu,[63,49] J.L. Liu,[64] J.Y. Liu,[1,54] K. Liu,[1] K.Y. Liu,[33] K. Liu,[6] L. Liu,[63,49] M.H. Liu,[9,f] P.L. Liu,[1] Q. Liu,[68] Q. Liu,[54] S.B. Liu,[63,49] S. Liu,[46] T. Liu,[1,54] T. Liu,[9,f] W.M. Liu,[63,49] X. Liu,[31,k,l] Y. Liu,[31,k,l] Y.B. Liu,[36] Z.A. Liu,[1,49,54] Z.Q. Liu,[41] X.C. Lou,[1,49,54] F.X. Lu,[50] H.J. Lu,[18] J.D. Lu,[1,54] J.G. Lu,[1,49] X.L. Lu,[1] Y. Lu,[1] Y.P. Lu,[1,49] C.L. Luo,[34] M.X. Luo,[70] P.W. Luo,[50] T. Luo,[9,f] X.L. Luo,[1,49] X.R. Lyu,[54] F.C. Ma,[33] H.L. Ma,[1] L.L. Ma,[41] M.M. Ma,[1,54] Q.M. Ma,[1] R.Q. Ma,[1,54] R.T. Ma,[54] X.X. Ma,[1,54] X.Y. Ma,[1,49] F.E. Maas,[15] M. Maggiora,[66A,66C] S. Maldaner,[4] S. Malde,[61] Q.A. Malik,[65] A. Mangoni,[23B] Y.J. Mao,[38,h] Z.P. Mao,[1] S. Marcello,[66A,66C] Z.X. Meng,[57] J.G. Messchendorp,[55] G. Mezzadri,[24A] T.J. Min,[35] R.E. Mitchell,[22] X.H. Mo,[1,49,54] N. Yu. Muchnoi,[10,b] H. Muramatsu,[59] S. Nakhoul,[11,d] Y. Nefedov,[29] F. Nerling,[11,d] I.B. Nikolaev,[10,b] Z. Ning,[1,49] S. Nisar,[8,g] S.L. Olsen,[54] Q. Ouyang,[1,49,54] S. Pacetti,[23B,23C] X. Pan,[9,f] Y. Pan,[58] A. Pathak,[1] A. Pathak,[27] P. Patteri,[23A] M. Pelizaeus,[4] H.P. Peng,[63,49] K. Peters,[11,d] J. Pettersson,[67] J.L. Ping,[34] R.G. Ping,[1,54] S. Pogodin,[29] R. Poling,[59] V. Prasad,[63,49] H. Qi,[63,49] H.R. Qi,[52] K.H. Qi,[25] M. Qi,[35] T.Y. Qi,[9] S. Qian,[1,49] W.B. Qian,[54] Z. Qian,[50] C.F. Qiao,[54] L.Q. Qin,[12]

JHEP11(2021)217

X.P. Qin,[9] X.S. Qin,[41] Z.H. Qin,[1,49] J.F. Qiu,[1] S.Q. Qu,[36] K.H. Rashid,[65] K. Ravindran,[21] C.F. Redmer,[28] A. Rivetti,[66C] V. Rodin,[55] M. Rolo,[66C] G. Rong,[1,54] Ch. Rosner,[15] M. Rump,[60] H.S. Sang,[63] A. Sarantsev,[29,c] Y. Schelhaas,[28] C. Schnier,[4] K. Schoenning,[67] M. Scodeggio,[24A,24B] D.C. Shan,[46] W. Shan,[19] X.Y. Shan,[63,49] J.F. Shangguan,[46] M. Shao,[63,49] C.P. Shen,[9] H.F. Shen,[1,54] P.X. Shen,[36] X.Y. Shen,[1,54] H.C. Shi,[63,49] R.S. Shi,[1,54] X. Shi,[1,49] X.D. Shi,[63,49] J.J. Song,[41] W.M. Song,[27,1] Y.X. Song,[38,h] S. Sosio,[66A,66C] S. Spataro,[66A,66C] K.X. Su,[68] P.P. Su,[46] F.F. Sui,[41] G.X. Sun,[1] H.K. Sun,[1] J.F. Sun,[16] L. Sun,[68] S.S. Sun,[1,54] T. Sun,[1,54] W.Y. Sun,[34] W.Y. Sun,[27] X. Sun,[20,i] Y.J. Sun,[63,49] Y.K. Sun,[63,49] Y.Z. Sun,[1] Z.T. Sun,[1] Y.H. Tan,[68] Y.X. Tan,[63,49] C.J. Tang,[45] G.Y. Tang,[1] J. Tang,[50] J.X. Teng,[63,49] V. Thoren,[67] W.H. Tian,[43] Y.T. Tian,[25] I. Uman,[53B] B. Wang,[1] C.W. Wang,[35] D.Y. Wang,[38,h] H.J. Wang,[31,k,l] H.P. Wang,[1,54] K. Wang,[1,49] L.L. Wang,[1] M. Wang,[41] M.Z. Wang,[38,h] M. Wang,[1,54] W. Wang,[50] W.H. Wang,[68] W.P. Wang,[63,49] X. Wang,[38,h] X.F. Wang,[31,k,l] X.L. Wang,[9,f] Y. Wang,[50] Y. Wang,[63,49] Y.D. Wang,[37] Y.F. Wang,[1,49,54] Y.Q. Wang,[1] Y.Y. Wang,[31,k,l] Z. Wang,[1,49] Z.Y. Wang,[1] Z. Wang,[54] Z. Wang,[1,54] D.H. Wei,[12] F. Weidner,[60] S.P. Wen,[1] D.J. White,[58] U. Wiedner,[4] G. Wilkinson,[61] M. Wolke,[67] L. Wollenberg,[4] J.F. Wu,[1,54] L.H. Wu,[1] L.J. Wu,[1,54] X. Wu,[9,f] Z. Wu,[1,49] L. Xia,[63,49] H. Xiao,[9,f] S.Y. Xiao,[1] Z.J. Xiao,[34] X.H. Xie,[38,h] Y.G. Xie,[1,49] Y.H. Xie,[6] T.Y. Xing,[1,54] C.J. Xu,[50] G.F. Xu,[1] Q.J. Xu,[14] W. Xu,[1,54] X.P. Xu,[46] Y.C. Xu,[54] F. Yan,[9,f] L. Yan,[9,f] W.B. Yan,[63,49] W.C. Yan,[71] X. Yan,[46] H.J. Yang,[42,e] H.X. Yang,[1] L. Yang,[43] S.L. Yang,[54] Y.X. Yang,[12] Y. Yang,[1,54] Z. Yang,[25] M. Ye,[1,49] M.H. Ye,[7] J.H. Yin,[1] Z.Y. You,[50] B.X. Yu,[1,49,54] C.X. Yu,[36] G. Yu,[1,54] J.S. Yu,[20,i] T. Yu,[64] C.Z. Yuan,[1,54] L. Yuan,[2] X.Q. Yuan,[38,h] Y. Yuan,[1] Z.Y. Yuan,[50] C.X. Yue,[32] A.A. Zafar,[65] X. Zeng Zeng,[6] Y. Zeng,[20,i] A.Q. Zhang,[1] B.X. Zhang,[1] G. Zhang,[16] H. Zhang,[63] H.H. Zhang,[27] H.H. Zhang,[50] H.Y. Zhang,[1,49] J.L. Zhang,[69] J.Q. Zhang,[34] J.W. Zhang,[1,49,54] J.Y. Zhang,[1] J.Z. Zhang,[1,54] J. Zhang,[1,54] J. Zhang,[1,54] L.M. Zhang,[52] L.Q. Zhang,[50] L. Zhang,[35] S. Zhang,[50] S.F. Zhang,[35] S. Zhang,[20,i] X.D. Zhang,[37] X.Y. Zhang,[41] Y. Zhang,[61] Y.T. Zhang,[71] Y.H. Zhang,[1,49] Y. Zhang,[63,49] Y. Zhang,[1] Z.Y. Zhang,[68] G. Zhao,[1] J. Zhao,[32] J.Y. Zhao,[1,54] J.Z. Zhao,[1,49] L. Zhao,[63,49] L. Zhao,[1] M.G. Zhao,[36] Q. Zhao,[1] S.J. Zhao,[71] Y.B. Zhao,[1,49] Y.X. Zhao,[25] Z.G. Zhao,[63,49] A. Zhemchugov,[29,a] B. Zheng,[64] J.P. Zheng,[1,49] Y.H. Zheng,[54] B. Zhong,[34] C. Zhong,[64] L.P. Zhou,[1,54] Q. Zhou,[1,54] X. Zhou,[68] X.K. Zhou,[54] X.R. Zhou,[63,49] X.Y. Zhou,[32] A.N. Zhu,[1,54] J. Zhu,[36] K. Zhu,[1] K.J. Zhu,[1,49,54] S.H. Zhu,[62] T.J. Zhu,[69] W.J. Zhu,[9,f] W.J. Zhu,[36] Y.C. Zhu,[63,49] Z.A. Zhu,[1,54] B.S. Zou,[1] J.H. Zou[1]

[1] *Institute of High Energy Physics, Beijing 100049, People's Republic of China*
[2] *Beihang University, Beijing 100191, People's Republic of China*
[3] *Beijing Institute of Petrochemical Technology, Beijing 102617, People's Republic of China*
[4] *Bochum Ruhr-University, Bochum D-44780, Germany*
[5] *Carnegie Mellon University, Pittsburgh, Pennsylvania 15213, U.S.A.*
[6] *Central China Normal University, Wuhan 430079, People's Republic of China*
[7] *China Center of Advanced Science and Technology, Beijing 100190, People's Republic of China*
[8] *COMSATS University Islamabad, Lahore Campus, Defence Road, Off Raiwind Road, 54000 Lahore, Pakistan*
[9] *Fudan University, Shanghai 200443, People's Republic of China*
[10] *G.I. Budker Institute of Nuclear Physics SB RAS (BINP), Novosibirsk 630090, Russia*
[11] *GSI Helmholtzcentre for Heavy Ion Research GmbH, Darmstadt D-64291, Germany*
[12] *Guangxi Normal University, Guilin 541004, People's Republic of China*
[13] *Guangxi University, Nanning 530004, People's Republic of China*
[14] *Hangzhou Normal University, Hangzhou 310036, People's Republic of China*
[15] *Helmholtz Institute Mainz, Staudinger Weg 18, Mainz D-55099, Germany*
[16] *Henan Normal University, Xinxiang 453007, People's Republic of China*

JHEP11(2021)217

[17] Henan University of Science and Technology, Luoyang 471003, People's Republic of China
[18] Huangshan College, Huangshan 245000, People's Republic of China
[19] Hunan Normal University, Changsha 410081, People's Republic of China
[20] Hunan University, Changsha 410082, People's Republic of China
[21] Indian Institute of Technology Madras, Chennai 600036, India
[22] Indiana University, Bloomington, Indiana 47405, U.S.A.
[23] INFN Laboratori Nazionali di Frascati , (A)INFN Laboratori Nazionali di Frascati, Frascati I-00044, Italy; (B)INFN Sezione di Perugia, Perugia I-06100, Italy; (C)University of Perugia, Perugia I-06100, Italy
[24] INFN Sezione di Ferrara, (A)INFN Sezione di Ferrara, Ferrara I-44122, Italy; (B)University of Ferrara, Ferrara I-44122, Italy
[25] Institute of Modern Physics, Lanzhou 730000, People's Republic of China
[26] Institute of Physics and Technology, Peace Ave. 54B, Ulaanbaatar 13330, Mongolia
[27] Jilin University, Changchun 130012, People's Republic of China
[28] Johannes Gutenberg University of Mainz, Johann-Joachim-Becher-Weg 45, Mainz D-55099, Germany
[29] Joint Institute for Nuclear Research, Dubna 141980, Moscow Region, Russia
[30] Justus-Liebig-Universitaet Giessen, II. Physikalisches Institut, Heinrich-Buff-Ring 16, Giessen D-35392, Germany
[31] Lanzhou University, Lanzhou 730000, People's Republic of China
[32] Liaoning Normal University, Dalian 116029, People's Republic of China
[33] Liaoning University, Shenyang 110036, People's Republic of China
[34] Nanjing Normal University, Nanjing 210023, People's Republic of China
[35] Nanjing University, Nanjing 210093, People's Republic of China
[36] Nankai University, Tianjin 300071, People's Republic of China
[37] North China Electric Power University, Beijing 102206, People's Republic of China
[38] Peking University, Beijing 100871, People's Republic of China
[39] Qufu Normal University, Qufu 273165, People's Republic of China
[40] Shandong Normal University, Jinan 250014, People's Republic of China
[41] Shandong University, Jinan 250100, People's Republic of China
[42] Shanghai Jiao Tong University, Shanghai 200240, People's Republic of China
[43] Shanxi Normal University, Linfen 041004, People's Republic of China
[44] Shanxi University, Taiyuan 030006, People's Republic of China
[45] Sichuan University, Chengdu 610064, People's Republic of China
[46] Soochow University, Suzhou 215006, People's Republic of China
[47] South China Normal University, Guangzhou 510006, People's Republic of China
[48] Southeast University, Nanjing 211100, People's Republic of China
[49] State Key Laboratory of Particle Detection and Electronics, Beijing 100049, Hefei 230026, People's Republic of China
[50] Sun Yat-Sen University, Guangzhou 510275, People's Republic of China
[51] Suranaree University of Technology, University Avenue 111, Nakhon Ratchasima 30000, Thailand
[52] Tsinghua University, Beijing 100084, People's Republic of China
[53] Turkish Accelerator Center Particle Factory Group, (A)Istinye University, Istanbul 34010, Turkey; (B)Near East University, Nicosia, North Cyprus, Mersin 10, Turkey
[54] University of Chinese Academy of Sciences, Beijing 100049, People's Republic of China
[55] University of Groningen, Groningen NL-9747 AA, The Netherlands
[56] University of Hawaii, Honolulu, Hawaii 96822, U.S.A.
[57] University of Jinan, Jinan 250022, People's Republic of China
[58] University of Manchester, Oxford Road, Manchester M13 9PL, United Kingdom
[59] University of Minnesota, Minneapolis, Minnesota 55455, U.S.A.
[60] University of Muenster, Wilhelm-Klemm-Str. 9, Muenster 48149, Germany
[61] University of Oxford, Keble Rd, Oxford OX13RH, U.K.
[62] University of Science and Technology Liaoning, Anshan 114051, People's Republic of China

JHEP11(2021)217

[63] University of Science and Technology of China, Hefei 230026, People's Republic of China
[64] University of South China, Hengyang 421001, People's Republic of China
[65] University of the Punjab, Lahore 54590, Pakistan
[66] University of Turin and INFN, (A)University of Turin, Turin I-10125, Italy; (B)University of Eastern Piedmont, Alessandria I-15121, Italy; (C)INFN, Turin I-10125, Italy
[67] Uppsala University, Box 516, Uppsala SE-75120, Sweden
[68] Wuhan University, Wuhan 430072, People's Republic of China
[69] Xinyang Normal University, Xinyang 464000, People's Republic of China
[70] Zhejiang University, Hangzhou 310027, People's Republic of China
[71] Zhengzhou University, Zhengzhou 450001, People's Republic of China
[a] Also at the Moscow Institute of Physics and Technology, Moscow 141700, Russia
[b] Also at the Novosibirsk State University, Novosibirsk 630090, Russia
[c] Also at the NRC "Kurchatov Institute", PNPI, Gatchina 188300, Russia
[d] Also at Goethe University Frankfurt, Frankfurt am Main 60323, Germany
[e] Also at Key Laboratory for Particle Physics, Astrophysics and Cosmology, Ministry of Education; Shanghai Key Laboratory for Particle Physics and Cosmology; Institute of Nuclear and Particle Physics, Shanghai 200240, People's Republic of China
[f] Also at Key Laboratory of Nuclear Physics and Ion-beam Application (MOE) and Institute of Modern Physics, Fudan University, Shanghai 200443, People's Republic of China
[g] Also at Harvard University, Department of Physics, Cambridge, MA 02138, U.S.A.
[h] Also at State Key Laboratory of Nuclear Physics and Technology, Peking University, Beijing 100871, People's Republic of China
[i] Also at School of Physics and Electronics, Hunan University, Changsha 410082, China
[j] Also at Guangdong Provincial Key Laboratory of Nuclear Science, Institute of Quantum Matter, South China Normal University, Guangzhou 510006, China
[k] Also at Frontiers Science Center for Rare Isotopes, Lanzhou University, Lanzhou 730000, People's Republic of China
[l] Also at Lanzhou Center for Theoretical Physics, Lanzhou University, Lanzhou 730000, People's Republic of China

JHEP11(2021)217